Global Crustal Thickness Revealed by Surface Waves Orbiting Mars

D. Kim, C. Duran, D. Giardini, A. -C. Plesa, S. C. Stähler, C. Boehm, V. Lekić, S. M. Mclennan, S. Ceylan, J. F. Clinton, et al.

Geophysical Research Letters

RESEARCH LETTER
10.1029/2023GL103482

Special Section:
The Large Marsquake of Sol 1222

Global Crustal Thickness Revealed by Surface Waves Orbiting Mars

D. Kim[1], C. Duran[1], D. Giardini[1], A.-C. Plesa[2], S. C. Stähler[1,3], C. Boehm[1], V. Lekić[4], S. M. McLennan[5], S. Ceylan[1], J. F. Clinton[6], P. Davis[7], A. Khan[8], B. Knapmeyer-Endrun[9,10], M. P. Panning[11], M. Wieczorek[12], P. Lognonné[12], and W. B. Banerdt[11]

[1]Institute of Geophysics, ETH Zurich, Zürich, Switzerland, [2]Institute of Planetary Research, German Aerospace Center (DLR), Berlin, Germany, [3]Physik-Institut, Universitä Zürich, Zürich, Switzerland, [4]Department of Geology, University of Maryland, College Park, MD, USA, [5]Department of Geosciences, Stony Brook University, Stony Brook, NY, USA, [6]Swiss Seismological Service, ETH Zurich, Zürich, Switzerland, [7]Department of Earth, Planetary, and Space Sciences, University of California Los Angeles, Los Angeles, CA, USA, [8]Institute of Geochemistry and Petrology, ETH Zurich, Zürich, Switzerland, [9]Bensberg Observatory, University of Cologne, Bergisch Gladbach, Germany, [10]Space Operations and Astronaut Training, German Aerospace Center (DLR), Cologne, Germany, [11]Jet Propulsion Laboratory, California Institute of Technology, Pasadena, CA, USA, [12]Université Paris Cité, Institut de physique du globe de Paris, CNRS, Paris, France

Key Points:

- We present the first observation of Rayleigh waves that orbit around Mars up to three times
- Group velocity measurements and 3-D simulations constrain the average crustal and uppermost mantle velocities along the great-circle propagation path
- The global average crustal thickness is 42–56 km and requires a large enrichment of heat-producing elements to explain local melt zones

Supporting Information:

Supporting Information may be found in the online version of this article.

Correspondence to:

D. Kim,
doyeon.kim@erdw.ethz.ch

Citation:

Kim, D., Duran, C., Giardini, D., Plesa, A.-C., Stähler, S. C., Boehm, C., et al. (2023). Global crustal thickness revealed by surface waves orbiting Mars. *Geophysical Research Letters*, *50*, e2023GL103482. https://doi.org/10.1029/2023GL103482

Received 28 FEB 2023
Accepted 28 APR 2023

Abstract We report observations of Rayleigh waves that orbit around Mars up to three times following the S1222a marsquake. Averaging these signals, we find the largest amplitude signals at 30 and 85 s central period, propagating with distinctly different group velocities of 2.9 and 3.8 km/s, respectively. The group velocities constraining the average crustal thickness beneath the great circle path rule out the majority of previous crustal models of Mars that have a >200 kg/m^3 density contrast across the equatorial dichotomy between northern lowlands and southern highlands. We find that the thickness of the Martian crust is 42–56 km on average, and thus thicker than the crusts of the Earth and Moon. Considered with the context of thermal evolution models, a thick Martian crust suggests that the crust must contain 50%–70% of the total heat production to explain present-day local melt zones in the interior of Mars.

Plain Language Summary The NASA InSight mission and its seismometer installed on the surface of Mars is retired after ∼4 years of operation. From the largest marsquake recording during the entire mission, we observe clear seismic signals from surface waves called Rayleigh waves that orbit around Mars up to three times. By measuring the wavespeeds with which these surface waves travel at different frequencies, we obtain the first seismic evidence that constrains the average crustal and uppermost mantle structures beneath the traveling path on a planetary scale. Using the new seismic observations together with gravity data, we confirm that the density of the crust in the northern lowlands and the southern highlands is similar, differing by no more than 200 kg/m^3. Furthermore, we find that the global average crustal thickness on Mars is 42–56 km, much thicker than the Earth's and Moon's crusts. By exploring Mars' thermal history, a thick Martian crust requires about 50%–70% of the heat-producing elements such as thorium, uranium, and potassium to be concentrated in the crust in order to explain local regions in the Martian mantle that can still undergo melting at present day.

1. Introduction

After more than 4 Earth years (∼1,450 sols) of operation on the Martian surface monitoring the planet's ground vibrations, the InSight mission (Banerdt et al., 2020) is now retired and its seismometer (SEIS, Lognonné et al., 2019) is no longer operating. Throughout the mission, analyses of body waves from marsquakes (Ceylan et al., 2022; Giardini et al., 2020; InSight Marsquake Service, 2022) and impacts (Garcia et al., 2022; Posiolova et al., 2022) have led to important discoveries about the planet's crust (Kim, Lekić, et al., 2021; Knapmeyer-Endrun et al., 2021; Lognonné et al., 2020), mantle (Drilleau et al., 2022; Durán et al., 2022; Khan et al., 2021), and core (Irving et al., 2023; Khan et al., 2022; Stähler et al., 2021). Recent detection of fundamental mode surface waves and overtones, together with gravimetric modeling enabled the characterization of crustal structure variations away from the InSight landing site and showed that the average crustal velocity and density structure is similar between the northern lowlands and the southern highlands (Kim, Banerdt, et al., 2022; Kim, Stähler, et al., 2022).

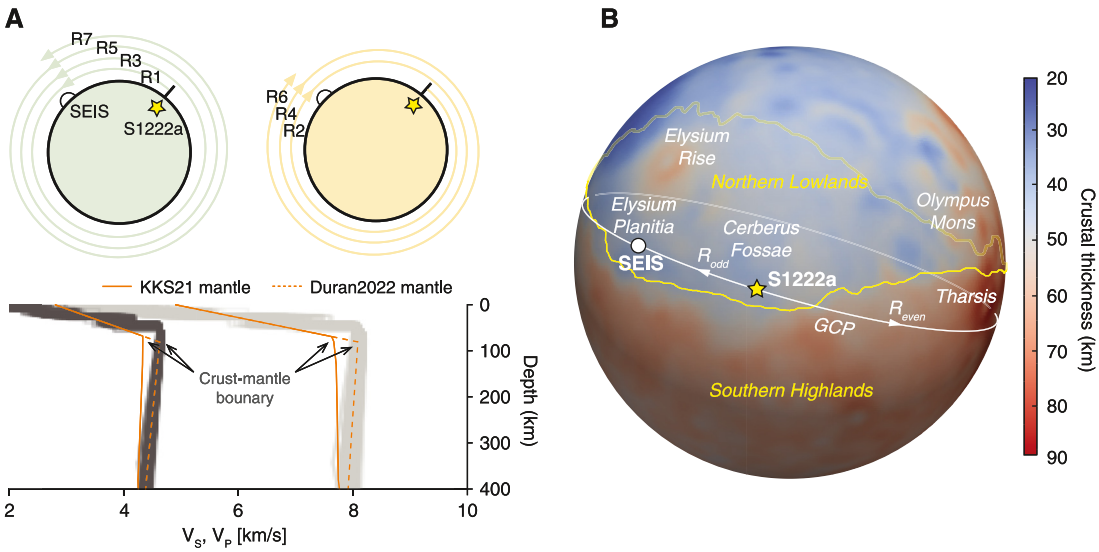

Figure 1. (a) Top diagram describes the direction of propagation and number of cycles for those surface waves orbiting around Mars in S1222a. Bottom shows 1-D interior models of Mars explored in this study. The crustal velocity profile constrained by previous surface wave studies are expanded to the existing mantle models of KKS21 (solid) and Duran2022 (dashed). For 3-D wavefield simulations, the two composite profiles are extrapolated by the thickness ranges shown in panel (b). Gray profiles are the posterior distribution of models in Durán et al. (2022). (b) Crustal thickness distribution between the northern lowlands and southern highlands on Mars. S1222a and the lander locations are denoted by yellow and white symbols, respectively. Background colormap denotes the crustal thickness used for generating our 3-D crustal velocity model of Mars. Dichotomy boundary (yellow line) is based on Andrews-Hanna et al. (2008). SEIS = InSight seismometer and GCP = Great circle path (white line).

Earlier in the mission, the InSight science team produced 1-D models of Mars' interior (KKS21; named after the three publications of Knapmeyer-Endrun et al. (2021), Khan et al. (2021), and Stähler et al. (2021)) by inverting travel times of the body wave arrivals together with geophysical and geodynamical parameters as a function of composition, temperature, and pressure at depth. Recently, cosmochemical constraints on the nature of the mantle (e.g., Khan et al., 2022) have been used to construct a unified description of the planetary structure that can explain both observed geophysical measurements as well as the major element distribution. Using an expanded body wave data set and the new mantle composition of Mars, updated 1-D interior models of the planet are now available (e.g., Durán et al., 2022).

Despite different approaches and the new compositional constraints incorporated into the modeling, more than 75% of the seismic body wave measurements are predominantly sensitive to the lithospheric structure between Elysium Planitia and Cerberus Fosse where most of the planet's seismicity (Stähler et al., 2022) and small meteorite impacts have been observed (Garcia et al., 2022). Similarly, in those 1-D models, crustal structure directly beneath the landing site of InSight is assumed to be representative of average Martian crust. These observational limitations and modeling choices can significantly bias our inferences of the global interior structure and dynamics of Mars.

In this study, we identify Rayleigh waves that orbit around Mars up to three times (up to R7; Figure 1a) and report their group velocity measurements for the largest seismic event recorded by InSight. By analyzing long- (LP) and very-long-period (VLP) R2-R7 energy and three-dimensional (3-D) wavefield simulations, we measure seismic wavespeeds in average crustal and mantle structures and improve previously reported estimates on global crustal thickness of Mars. We highlight the implications of the new constraints from our analysis for the planet's interior structure and thermal evolution.

2. Data and Methods

2.1. Seismic Analysis of S1222a

The largest seismic event detected during the InSight mission is the M_W^{ma} 4.6 marsquake S1222a (InSight Marsquake Service, 2023; Kawamura et al., 2022) (Figure 1b). The seismic waveforms of S1222a contain both minor-arc Rayleigh and Love waves (e.g., Beghein et al., 2022), overtones (Kim, Stähler, et al., 2022), and

Rayleigh waves that propagate around Mars for one cycle (R2 and R3) (e.g., Panning et al., 2023). To extend our analysis and search for Rayleigh waves traveling multiple times around Mars, we consider a 10-hr long seismic recording of S1222a (InSight Marsquake Service, 2023) (Figure S1 in Supporting Information S1). We apply marsquake seismic data processing techniques to remove electro-mechanical noise by the sensor and the lander (Scholz et al., 2020), to suppress spurious signals and to avoid misinterpretation of the SEIS data (Kim, Davis, et al., 2021). We restrict our analysis to the 25–100 s period range because seismic energy observed outside this frequency range can be affected by atmospheric turbulence at various scales at longer periods (Banfield et al., 2020) or overprinted by strong scattering at shorter periods (Karakostas et al., 2021; van Driel et al., 2021). We correct for the presence of scattered waves in the seismic coda by examining frequency dependent polarization attributes (FDPAs) (e.g., Park et al., 1987) (see Text S1 in Supporting Information S1 for more details). To further enhance the signal-to-noise ratio of our data, we take ±200 s of the predicted R2-R7 arrival times and perform a *N*th root stacking ($N = 4$) assuming that waves propagate along the great circle path (GCP), a commonly made assumption in surface wave analysis on Earth (e.g., Moulik et al., 2022). We consider a range of GCPs based on the back azimuth uncertainties of the direct *P*-, *S*-waves, and minor-arc surface waves (Kawamura et al., 2022; Kim, Stähler, et al., 2022; Panning et al., 2023). Prediction windows for Rayleigh wave travel times are computed according to the depth sensitivity for each period range and the KKS21 model. The minor-arc Rayleigh wave (R1) is not included in the analysis to avoid producing a bias toward the minor-arc path. Here, we use the envelope rather than the waveform to prevent distortion of seismic signals produced by nonlinear processing (e.g., Rost & Thomas, 2002).

2.2. 3-D Wavefield Simulation of S1222a

Previously, little deviation for R1–R3 travel times in S1222a between the GCP and the ray theoretical path has been reported for existing crustal thickness models of Mars (Kim, Stähler, et al., 2022). To account for more realistic volumetric sensitivities for higher-orbit Rayleigh wave propagation with existing crustal thickness variations on Mars, we carry out a 3-D wavefield simulation using the spectral-element code by Afanasiev et al. (2019). For our input model, we employ the 3-D crustal velocity modeling scheme used in the analysis of 3-D ray tracing by Kim, Stähler et al. (2022). The initial crustal velocity profile is characterized by a positive velocity gradient of 0.02 km/s per km with an average shear velocity (V_S) of 3.2 km/s based on previous surface wave analyses of S1222a and the two large impacts, S1094b and S1000a (Figure 1a). Within the crustal layer, we extrapolated and vertical scaled the velocity profile based on the distribution of crustal thicknesses (e.g., Figure 1b). For the mantle, we consider: (a) the 1-D reference velocity model of KKS21 (solid, Figure 1a) and (b) the recently updated 1-D models that have a 5% faster uppermost mantle velocity resulting from a reduced mantle FeO content (hereafter Duran2022; dashed, Figure 1a). See Text S2 in Supporting Information S1 for more details.

3. Results and Discussion

Our LP (∼30 s) vertical-component envelope shows strong amplitude signals in the predicted time windows for R1, R2, and R3 traveling with an average group velocity range of 2.4–3.0 km/s (black curve, Figure 2a). We observe weaker and more localized later-arrivals within the predicted time windows for R4–R7, which appear to have relatively large elliptically polarized energy in the vertical plane in the same period range as expected for Rayleigh waves (dashed brown, Figure 2a). Conversely, linearly polarized signals such as a small amplitude glitch (gray, Figure 2a) or other body wave arrivals show a negative correlation between envelope amplitude and the polarization. In the case of VLP (∼85 s), the envelope amplitude and the corresponding FDPA curve is highly correlated and both data show distinctive peaks observed across the predicted windows with a higher traveling speed of 3.6–4.0 km/s (Figure 2b). For both period ranges, we observe statistically significant correlations between seismic observables within the R2–R7 windows above 99% confidence level (Figure S2 in Supporting Information S1) (see also Text S3 in Supporting Information S1 for more details). Arrivals outside the predicted windows for LP and VLP data could be due to multipathing of the propagated surface waves in 3-D crustal structure or body-to-surface wave conversion. Averaging across the R2–R7 signals, we observe the strongest amplitude signals at 30 and 85 s central periods, propagating with distinctively different group velocities of 2.9 and 3.8 km/s, respectively, in both amplitude and polarization stacks (Figures 2c and 2d).

Although similar group velocities have been independently reported by other studies for R2 and R3 arrivals in S1222a at 30 s (Kim, Stähler, et al., 2022; Li et al., 2022; Panning et al., 2023), the observed group velocities

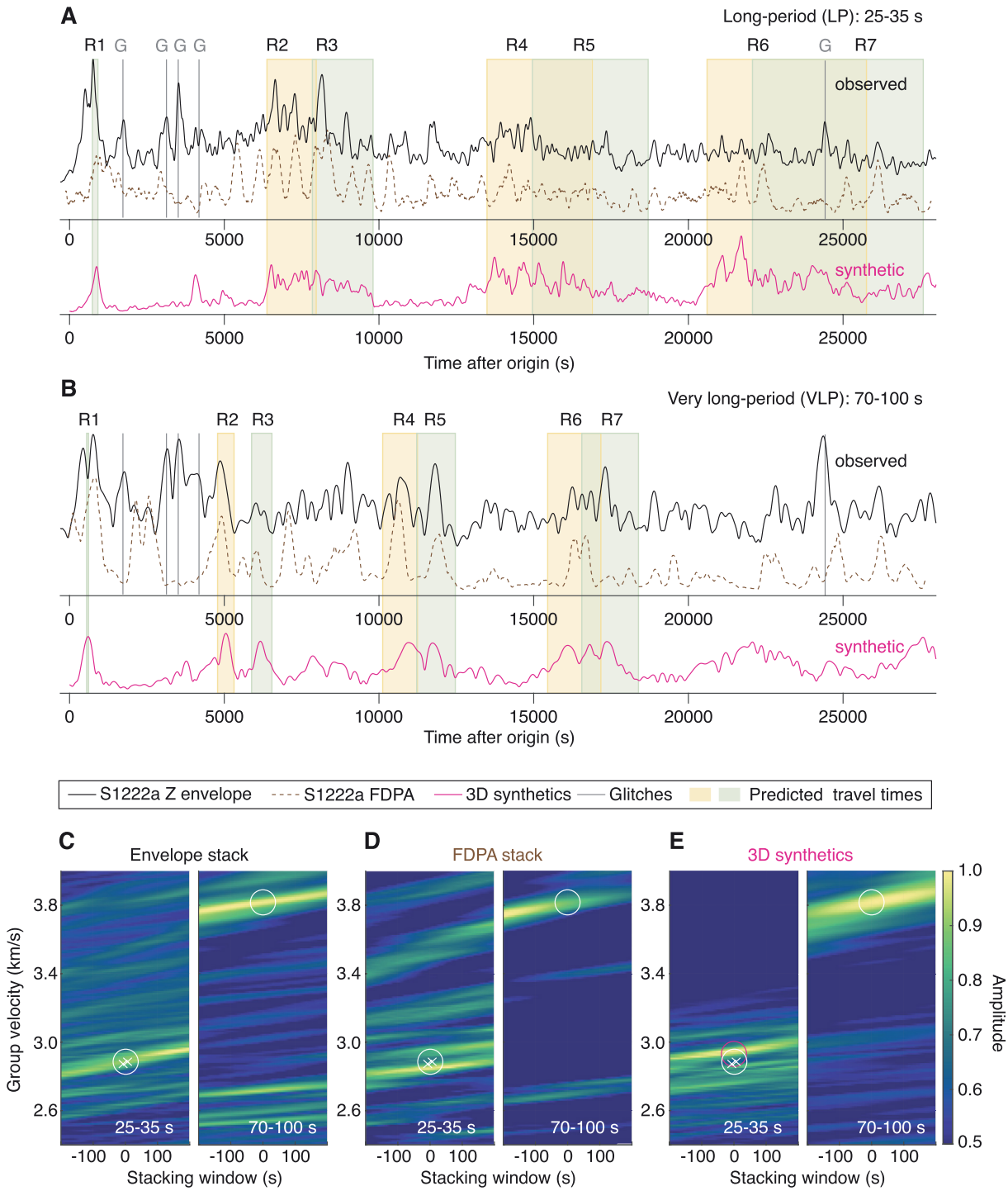

Figure 2. Vertical-component envelopes of the S1222a deglitched waveform (black) and the FDPAs for elliptically polarized particle motion in vertical plane (dashed brown) filtered between (a) 25–35 s (LP) and (b) 70–100 s periods (very-long-period [VLP]). Shaded areas indicate the predicted time windows of R1–R7 arrivals base on the group velocities ranging from 2.4 to 3.0 to 3.6–4.0 km/s for LP and VLP data, respectively. Glitches are shown by gray lines. Envelopes in magenta are based on a 3-D wavefield simulation using the model with crustal thickness variation shown in Figure 1. Group velocity measurements of R2–R7 are obtained by Nth-root stacking of the time-series in (a, b) for (c, d) data and (e) synthetics. White crosses are from independent analyses of R2 and R3 by Kim, Stähler et al. (2022). White and magenta circles denote the largest amplitude signals observed at the center of 400 s long stacking window for data and synthetics, respectively. See Figure S3 in Supporting Information S1 for the complete analysis between 25 and 100 s with narrow-band filters. G = glitches and FDPA = frequency dependent polarization attribute.

show an apparent jump at intermediate periods between 20 and 100 s (Figure S3 in Supporting Information S1), unlike typical, smoothly varying surface wave dispersion curves, as predicted by the existing 1-D models (e.g., Drilleau et al., 2022; Durán et al., 2022) (Figure S4 in Supporting Information S1). Such abruptness in dispersion and the observed low and high velocities from the R2–R7 signals (Figure S3 in Supporting Information S1) cannot be solely attributed to elliptically polarized martian wind (e.g., Stutzmann et al., 2021) contaminating the data which is unlikely to be recorded with the apparent periodicity for both LP and VLP data. At much longer periods between 100 and 200 s, a similar group velocity close to 3.8 km/s for the excitation of R2 has been reported by using ambient noise correlations (Deng & Levander, 2022). A normal mode study on Mars has also shown some potential excitation of the fundamental mode surface waves in comparable period ranges between 120 and 300 s (Lognonné et al., 2023).

The predicted dispersion curves using a suite of 1-D models with varying crustal thickness illustrate that the two end-member group velocities at LP and VLP appear as a type of stationary phase or "Airy-phase" (Aki & Richards, 2002) across different periods (Figure S5 in Supporting Information S1). Depending on crustal thickness in a model, however, the shape of group velocity dispersion curves at intermediate periods will vary substantially and would not allow seismic signals associated with the surface waves to constructively interfere across multiple orbits of Mars. Such Airy-phase is often associated with the amplification of Rayleigh waves on Earth that can propagate for considerable distances across the continental crust (Ewing & Press, 1956) and mantle (Ewing & Press, 1954), mainly observed at 15–20 and 140–200 s, respectively. The observation of Rayleigh waves traveling over multiple orbits on the seismic recording of a relatively small-magnitude quake (M_W^{ma} 4.6) suggests those stationary values of group velocities on Mars could be occurring close to 30 and 85 s central periods.

Our 3-D wavefield simulations also show that large-scale variations in crustal thickness across the equatorial dichotomy are necessary to reproduce this behavior (Figures S6 and S7 in Supporting Information S1). Using our 3-D model, we find that the spectrum of the R2-R7 arrivals in synthetic waveform is largely discontinuous in time and frequency. This feature becomes more evident for Rayleigh waves propagating in higher-orbits beyond R3. The variation in amplitude of surface waves propagating toward the minor-arc versus major-arc directions (i.e., R_{odd} vs. R_{even}) also supports the evidence for lateral variation in crustal structure, likely due to (de)focusing of those waves (e.g., Romanowicz, 1987). Therefore, our observation of the absence of dispersion between ~30–85 s for R2–R7 in S1222a and their associated amplitude change substantiate the choice of our 3-D model with large variation in crustal thickness (i.e., 20–90 km) (Figure 1b) as these observations cannot be explained by existing 1-D models assuming a constant crustal thickness (Figure S4 in Supporting Information S1).

The group velocity obtained for the largest amplitudes seen in the synthetic LP stack is consistent with our R2–R7 measurement of ~2.9 km/s at ~30 s (with a small uncertainty of <2%; c. f., white and magenta symbols) (Figure 2e), indicating that the average speed at which R2–R7 travel within the crust can be well-recovered with our 3-D model even with a large variation in crustal thickness (e.g., Figure 1b). For the synthetic VLP stack, we find that the observed group velocity is strongly dependent on the versions of 1-D mantle models implemented in our analysis since the sensitivity of 70–100 s Rayleigh waves on Mars is predominantly between 75 and 115 km, a depth range in the uppermost mantle (Figure S8 in Supporting Information S1). For example, the recent 1-D models produced by Durán et al. (2022) or Drilleau et al. (2022) have a 5% faster uppermost mantle than KKS21 (Figure 1a). Our R2-R7 measurements are better fit by the newer sets of models that are based on a lower mantle FeO content compared to the KKS21 model that uses Wänke-Dreibus (Wänke et al., 1994) or Taylor compositions (Taylor, 2013) (c.f., Figure 2e and Figure S9 in Supporting Information S1). This difference in seismic wavespeeds in existing models of the uppermost mantle, however, does not significantly affect body wave travel times with limited sensitivity and geographical coverage nor the estimated event locations (Figure S10 in Supporting Information S1) (See also Text S4 in Supporting Information S1). Therefore, the new observations of R2–R7 provide a promising means of refining the 1-D models of the planet's radially symmetric structure, verifying the major element distribution of the Martian mantle and determining the crustal thickness variations.

To find the average crustal thickness along the GCP from S1222a to the InSight lander, we carry out a systematic model-space search seeking average crustal V_S, thickness, and uppermost mantle V_S that fit the observed velocities of R2–R7 (Figure 3a). We obtain a distribution of allowable velocities and thicknesses, with mean V_S of 3.38 km/s and 4.41 km/s for crustal and uppermost mantle, respectively, and a mean crustal thickness of 50 km beneath the GCP with an interquartile range between 44 and 58 km (magenta, Figure 3a). This estimate

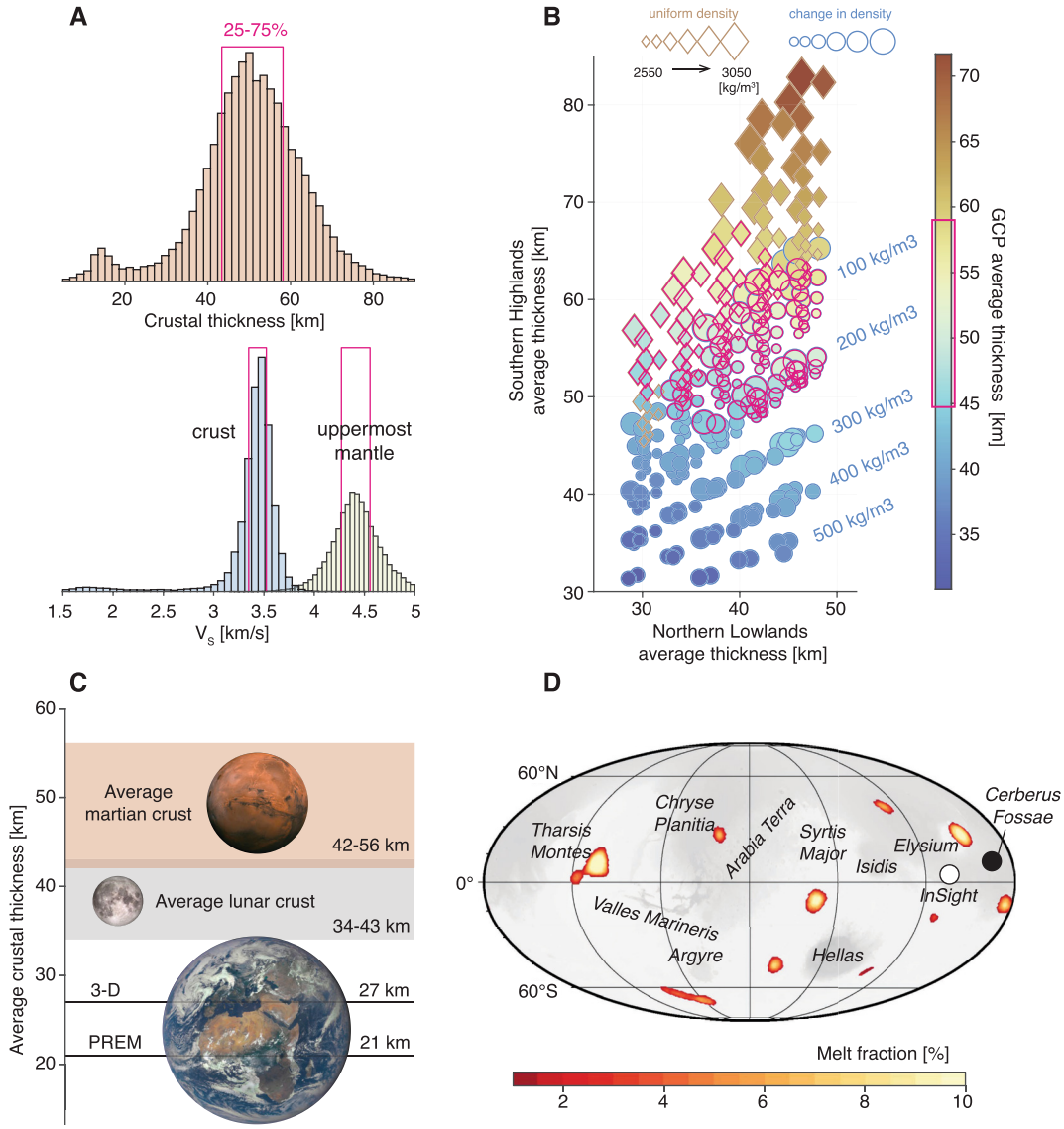

Figure 3. (a) Posterior distribution of the crustal and mantle V_S and crustal thickness along the great circle path (GCP) of S1222a. Interquartile range of the distribution is shown by red outlines. (b) Average crustal thickness of northern lowlands versus southern highlands for global crustal thickness models with crustal densities ranging from 2,550 to 3,050 kg/m^3 with (circle symbol) and without a density contrast (diamond symbol) across the dichotomy. Size of the symbol increases with increasing background crustal density values. Dichotomy boundary is based on Andrews-Hanna et al. (2008). Colormap denotes the mean crustal thickness along the GCP for each model. Those models within the red outline are compatible with the posterior distribution in panel (a). (c) New global average crustal thickness range obtained by the model selection in panel (b) in comparison to that of the Earth and the Moon where constraints based on seismic data are available. (d) Best-fitting thermal evolution model of Plesa et al. (2018) computed with the new crustal constraint in panel (c) and contain 53% of the total bulk content of radioactive elements in the crust. This model has average crustal densities of 2,750 and 2,550 kg/m^3 for northern lowlands and southern highlands, respectively, and an average global crustal thickness of 48 km. See Figures S11 and S12 in Supporting Information S1 for the rest of models with different sets of input parameters. PREM = Preliminary Reference Earth Model. 3-D = a global 3-D model by Huang et al. (2013).

of GCP-averaged crustal thickness and its uncertainty can be used as a robust anchoring-point and extrapolated globally using the existing models of crustal thickness based on gravimetric modeling (Wieczorek et al., 2022), which on their own suffer from a trade-off between average crustal density and thickness.

Crustal thickness directly beneath the lander based on RF analyses (Kim, Lekić, et al., 2021; Knapmeyer-Endrun et al., 2021) has previously been used as an anchoring-point to yield estimates of the average crustal thickness

on Mars in the 30–72 km range. Using the interquartile range of crustal thickness distribution along the GCP constrained by the R2–R7 analysis (magenta lines, Figure 3a) against those from all plausible models considered in this study (see Text S5 in Supporting Information S1), we were able to improve estimates of the average crustal thickness by ruling out the majority of those crustal models that have a >200 kg/m^3 density contrast across the dichotomy (Figure 3b). As a result, we obtain an estimate of the global average crustal thickness range between 42 and 56 km from the remaining models (symbols in magenta, Figure 3b), which is a significantly narrower range than previously available. This implies large differences in crustal thickness between the northern lowlands and the southern highlands (up to ∼30 km), and places new constraints on the average global thickness of the Martian crust, evidently thicker than the terrestrial (Dziewonski & Anderson, 1981; Huang et al., 2013) and the lunar crusts (Wieczorek et al., 2013) (Figure 3c).

Of the major rocky bodies in the inner solar system for which constraints are available, Mars very likely has the thickest crust (i.e., 42–56 km). Based largely on seismic data, Earth's crust averages only about 21 km (Dziewonski & Anderson, 1981) or 27 km in thickness (Huang et al., 2013). The thickness of the lunar crust, which is anchored by Apollo seismic data, is in the range of 34–43 km (Wieczorek et al., 2013) (Figure 3c). For the other bodies, there are no seismic data and crustal thickness constraints are based solely on gravity and topography measurements. Nevertheless, it is likely that on average, the thickness of the Venusian crust is in the range of about 8–26 km (James et al., 2013; Maia & Wieczorek, 2022) and the Mercurian crust in the range of 17–53 km (Padovan et al., 2015) or possibly even thinner (15–37 km, Sori, 2018). Even the crust of 4-Vesta may be broadly in this range with one estimate at 24 km (Ermakov et al., 2014). Accordingly, variations in crustal thicknesses of these rocky bodies appear to be within a factor of about 3–4 (McLennan, 2022). This is in contrast to planetary crustal masses which vary by well over an order of magnitude relative to the size of their respective primitive mantles, between about 0.6% for Venus (and a similar value of 0.7% for Earth, Huang et al., 2013) to as much as 9.5% for Mercury and 14% for 4-Vesta (McLennan, 2022). Our results are consistent with Mars being intermediate among these values with the crust representing about 4%–5% of the primitive mantle mass. Therefore, the degree of silicate differentiation into planetary crusts is more a function of overall planetary size than of crustal thickness and smaller bodies tend to have thicker crusts and increased degrees of mantle processing to form those crusts (McLennan, 2022; O'Rourke & Korenaga, 2012).

The tighter constraints on the crustal thickness obtained here compared to previously derived values from the RF analysis (Knapmeyer-Endrun et al., 2021) provide important information for thermal evolution models of the interior of Mars (Khan et al., 2021; Knapmeyer-Endrun et al., 2021; Plesa et al., 2018, 2021, 2022). Together, this can help to further refine the present-day temperature distribution and amount of heat-producing elements within the crust. Thermal evolution models produced by using a maximum density contrast of <200 kg/m^3 across the dichotomy constrained by the R2–R7 analysis show that more than half but less than 70% of the total radiogenic heat production needs to be in the crust. The decay of radioactive isotopes of Th, U, and K is the main source of heat in the interior of Mars today and while the models include other heat sources such as the heating by the core, their contribution is expected to be negligible at present day for Mars and other stagnant lid planets (e.g., Breuer & Moore, 2007). The high crustal enrichment on HPE we infer is required in order to produce local melt zones in the mantle at present day (see Figures S11 and S12 and Text S6 in Supporting Information S1 for more details). The inferred crustal heat production range is consistent with the study of Knapmeyer-Endrun et al. (2021). For three end-member crustal models tested in Figures S11 and S12 in Supporting Information S1, we obtained enrichment factors between 8.2 and 14.3 (corresponding to a crustal heat production of 46.7–64.4 pW/kg). These enrichment factors are close to, but extend to slightly larger values than the enrichment estimated from GRS data 8–10.3 (crustal heat production of 46–51 pW/kg; Hahn et al., 2011). Interestingly, our best-fitting model with a 200 kg/m^3 density contrast favors mantle plumes that can produce melt up to the present day close to Cerberus Fosse (inset, Figure 3d), supporting the interpretation from gravity and topography data (Broquet & Andrews-Hanna, 2022) and from seismic observations (Stähler et al., 2022). Therefore, our study offers a promising opportunity for further evaluating the plume hypothesis beneath Cerberus Fosse.

4. Conclusions

We present the observation of Rayleigh waves that orbit around Mars up to three times (R2–R7) using the InSight seismic recording of the largest marsquake of S1222a. Our analysis revealed that these Rayleigh waves are traveling with stationary group velocities of 2.9 and 3.8 km/s at 30 and 85 s central periods, respectively; energy at

intermediate periods does not appear to constructively interfere across multiple traveling cycles around Mars. 3-D wavefield simulations show that the presence of large-scale variations in crustal thickness across the equatorial dichotomy is necessary to reproduce this behavior. The observed group velocities further highlight the difference in radial profiles of seismic wavespeeds in existing models of the uppermost mantle, which are based on body wave travel times with limited sensitivity and geographical coverage. We find that previous crustal models of Mars with a >200 kg/m^3 density contrast across the dichotomy cannot explain the average crustal thickness beneath the GCP constrained by the R2–R7 group velocities. This implies large differences in crustal thickness between the northern lowlands and southern highlands, with the average global thickness of Martian crust estimated to be 42–56 km, which is thicker than the crusts on the Earth and Moon. Our study places new constraints on our understanding of the internal structure and evolution of Mars, and have implications for the potential existence of underlying plumes and local melt zones, such as Cerberus Fosse.

Data Availability Statement

The InSight event catalog https://doi.org/10.12686/a21 and waveform data are available from the IRIS-DMC http://ds.iris.edu/ds/nodes/dmc/tools/mars-events/, NASA-PDS https://pds-geosciences.wustl.edu/missions/insight/seis.htm and IPGP data center https://doi.org/10.18715/SEIS.INSIGHT.XB_2016.

Acknowledgments
This paper is InSight contribution number 315. The authors acknowledge the NASA, the CNES, their partner agencies and Institutions (UKSA, SSO, DLR, JPL, IPGP-CNRS, ETHZ, IC, and MPS-MPG) and the flight operations team at JPL, SISMOC, MSDS, IRIS-DMC, and PDS for providing the SEED SEIS data. Marsquake Service (MQS) operations at ETH are supported by ETH Research Grant ETH-06 17-02. ETH authors recognize support from the ETH + funding scheme (ETH+02 19-1: "Planet Mars"). A.-C.P. gratefully acknowledges the financial support and endorsement from the DLR Management Board Young Research Group Leader Program and the Executive Board Member of Space Research and Technology. V.L. acknowledge funding from NASA Grant 80NSSC18K1628 and NASA Solar System Exploration Research Virtual Institute (SSERVI) Cooperative Agreement 80NSSC19M0216. S.M.M. acknowledges funding from NASA Grant 80NSSC18K1622. D.K. thanks Adrien Broquet and Jeff Andrews-Hanna for insightful discussions. We acknowledge the thorough and thoughtful reviews from Barbara Romanowicz and an anonymous reviewer that greatly improved the manuscript.

References

Afanasiev, M., Boehm, C., van Driel, M., Krischer, L., Rietmann, M., May, D. A., et al. (2019). Modular and flexible spectral-element waveform modelling in two and three dimensions. *Geophysical Journal International*, *216*(3), 1675–1692. https://doi.org/10.1093/gji/ggy469

Aki, K., & Richards, P. G. (2002). *Quantitative seismology* (2nd ed.). University Science Books.

Andrews-Hanna, J. C., Zuber, M. T., & Banerdt, W. B. (2008). The borealis basin and the origin of the Martian crustal dichotomy. *Nature*, *453*(7199), 1212–1215. https://doi.org/10.1038/nature07011

Banerdt, W. B., Smrekar, S. E., Banfield, D., Giardini, D., Golombek, M., Johnson, C. L., et al. (2020). Initial results from the insight mission on Mars. *Nature Geoscience*, *13*(3), 183–189. https://doi.org/10.1038/s41561-020-0544-y

Banfield, D., Spiga, A., Newman, C., Forget, F., Lemmon, M., Lorenz, R., et al. (2020). The atmosphere of Mars as observed by insight. *Nature Geoscience*, *13*(3), 190–198. https://doi.org/10.1038/s41561-020-0534-0

Beghein, C., Li, J., Weidner, E., Maguire, R., Wookey, J., Lekić, V., et al. (2022). Crustal anisotropy in the Martian lowlands from surface waves. *Geophysical Research Letters*, *49*(24), e2022GL101508. https://doi.org/10.1029/2022gl101508

Breuer, D., & Moore, W. (2007). Dynamics and thermal history of the terrestrial planets, the moon, and IO. Planets and moons. *Treatise on geophysics*, *10*, 299–348.

Broquet, A., & Andrews-Hanna, J. C. (2022). Geophysical evidence for an active mantle plume underneath Elysium Planitia on Mars. *Nature Astronomy*, *7*(2), 1–10. https://doi.org/10.1038/s41550-022-01836-3

Ceylan, S., Clinton, J. F., Giardini, D., Stähler, S. C., Horleston, A., Kawamura, T., et al. (2022). The marsquake catalogue from insight, sols 0–1011. *Physics of the Earth and Planetary Interiors*, *333*, 106943. https://doi.org/10.1016/j.pepi.2022.106943

Deng, S., & Levander, A. (2022). Autocorrelation R2 on Mars. *Geophysical Research Letters*, *49*(17), e2022GL099580. https://doi.org/10.1029/2022gl099580

Drilleau, M., Samuel, H., Garcia, R. F., Rivoldini, A., Perrin, C., Michaut, C., et al. (2022). Marsquake locations and 1-D seismic models for Mars from insight data. *Journal of Geophysical Research: Planets*, *127*(9), e2021JE007067. https://doi.org/10.1029/2021je007067

Durán, C., Khan, A., Ceylan, S., Zenhäusern, G., Staehler, S., Clinton, J., & Giardini, D. (2022). Seismology on Mars: An analysis of direct, reflected, and converted seismic body waves with implications for interior structure. *Physics of the Earth and Planetary Interiors*, *325*, 106851. https://doi.org/10.1016/j.pepi.2022.106851

Dziewonski, A. M., & Anderson, D. L. (1981). Preliminary reference Earth model. *Physics of the Earth and Planetary Interiors*, *25*(4), 297–356. https://doi.org/10.1016/0031-9201(81)90046-7

Ermakov, A. I., Zuber, M. T., Smith, D. E., Raymond, C. A., Balmino, G., Fu, R. R., & Ivanov, B. A. (2014). Constraints on Vesta's interior structure using gravity and shape models from the dawn mission. *Icarus*, *240*, 146–160. https://doi.org/10.1016/j.icarus.2014.05.015

Ewing, M., & Press, F. (1954). An investigation of mantle Raleigh waves. *Bulletin of the Seismological Society of America*, *44*(2A), 127–147. https://doi.org/10.1785/bssa04402a0127

Ewing, M., & Press, F. (1956). Rayleigh wave dispersion in the period range 10 to 500 seconds. *Eos, Transactions American Geophysical Union*, *37*(2), 213–215. https://doi.org/10.1029/tr037i002p00213

Garcia, R. F., Daubar, I. J., Beucler, É., Posiolova, L. V., Collins, G. S., Lognonné, P., et al. (2022). Newly formed craters on Mars located using seismic and acoustic wave data from insight. *Nature Geoscience*, *15*(10), 774–780. https://doi.org/10.1038/s41561-022-01014-0

Giardini, D., Lognonné, P., Banerdt, W. B., Pike, W. T., Christensen, U., Ceylan, S., et al. (2020). The seismicity of Mars. *Nature Geoscience*, *13*(3), 205–212. https://doi.org/10.1038/s41561-020-0539-8

Hahn, B., McLennan, S., & Klein, E. (2011). Martian surface heat production and crustal heat flow from Mars Odyssey Gamma-Ray spectrometry. *Geophysical Research Letters*, *38*(14), L14203. https://doi.org/10.1029/2011gl047435

Huang, Y., Chubakov, V., Mantovani, F., Rudnick, R. L., & McDonough, W. F. (2013). A reference Earth model for the heat-producing elements and associated geoneutrino flux. *Geochemistry, Geophysics, Geosystems*, *14*(6), 2003–2029. https://doi.org/10.1002/ggge.20129

InSight Marsquake Service. (2022). Mars Seismic catalogue, InSight mission V3 2020-07-01 [Dataset]. ETHZ, IPGP, JPL, ICL, ISAE-Supaero, MPS. Univ Bristol. https://doi.org/10.12686/a19

InSight Marsquake Service. (2023). *Mars seismic catalogue, insight mission; v14 2023-04-01*. ETHZ, IPGP, JPL, ICL, Univ. Bristol. Retrieved from https://www.insight.ethz.ch/seismicity/catalog/v14/

Irving, J. C. E., Lekic, V., Duran, C., Drilleau, M., Kim, D., Rivoldini, A., et al. (2023). First observations of core-transition seismic phases on Mars. *Proceedings of the National Academy of Sciences*, *120*(18), e2217090120. https://doi.org/10.1073/pnas.2217090120

James, P. B., Zuber, M. T., & Phillips, R. J. (2013). Crustal thickness and support of topography on Venus. *Journal of Geophysical Research: Planets*, *118*(4), 859–875. https://doi.org/10.1029/2012je004237

Karakostas, F., Schmerr, N., Maguire, R., Huang, Q., Kim, D., Lekic, V., et al. (2021). Scattering attenuation of the Martian interior through coda-wave analysis. *Bulletin of the Seismological Society of America*, *111*(6), 3035–3054. https://doi.org/10.1785/0120210253

Kawamura, T., Clinton, J. F., Zenhäusern, G., Ceylan, S., Horleston, A. C., Dahmen, N. L., et al. (2022). S1222a - The largest marsquake detected by insight. *Geophysical Research Letters*, *50*(5), e2022GL101543. https://doi.org/10.1029/2022GL101543

Khan, A., Ceylan, S., van Driel, M., Giardini, D., Lognonné, P., Samuel, H., et al. (2021). Upper mantle structure of Mars from insight seismic data. *Science*, *373*(6553), 434–438. https://doi.org/10.1126/science.abf2966

Khan, A., Sossi, P. A., Liebske, C., Rivoldini, A., & Giardini, D. (2022). Geophysical and cosmochemical evidence for a volatile-rich Mars. *Earth and Planetary Science Letters*, *578*, 117330. https://doi.org/10.1016/j.epsl.2021.117330

Kim, D., Banerdt, W., Ceylan, S., Giardini, D., Lekić, V., Lognonné, P., et al. (2022). Surface waves and crustal structure on Mars. *Science*, *378*(6618), 417–421. https://doi.org/10.1126/science.abq7157

Kim, D., Davis, P., Lekić, V., Maguire, R., Compaire, N., Schimmel, M., et al. (2021). Potential pitfalls in the analysis and structural interpretation of seismic data from the Mars insight mission. *Bulletin of the Seismological Society of America*, *111*(6), 2982–3002. https://doi.org/10.1785/0120210123

Kim, D., Lekić, V., Irving, J. C., Schmerr, N., Knapmeyer-Endrun, B., Joshi, R., et al. (2021). Improving constraints on planetary interiors with PPS receiver functions. *Journal of Geophysical Research: Planets*, *126*(11), e2021JE006983. https://doi.org/10.1029/2021je006983

Kim, D., Stähler, S., Ceylan, S., Lekic, V., Maguire, R., Zenhäusern, G., et al. (2022). Structure along the Martian dichotomy constrained by Raleigh and love waves and their overtones. *Geophysical Research Letters*, *50*, e2022GL101666. https://doi.org/10.1029/2022GL101666

Knapmeyer-Endrun, B., Panning, M. P., Bissig, F., Joshi, R., Khan, A., Kim, D., et al. (2021). Thickness and structure of the Martian crust from insight seismic data. *Science*, *373*(6553), 438–443. https://doi.org/10.1126/science.abf8966

Li, J., Beghein, C., Lognonné, P., McLennan, S. M., Wieczorek, M., Panning, M., et al. (2022). Different Martian crustal seismic velocities across the dichotomy boundary from multi-orbiting surface waves. *Geophysical Research Letters*, *50*(1), e2022GL101243. https://doi.org/10.1029/2022GL101243

Lognonné, P., Banerdt, W., Pike, W., Giardini, D., Christensen, U., Garcia, R., et al. (2020). Constraints on the shallow elastic and anelastic structure of Mars from InSight seismic data. *Nature Geoscience*, *13*(3), 213–220. https://doi.org/10.1038/s41561-020-0536-y

Lognonné, P., Banerdt, W. B., Giardini, D., Pike, W. T., Christensen, U., Laudet, P., et al. (2019). SEIS: Insight's seismic experiment for internal structure of Mars. *Space Science Reviews*, *215*, 1–170. https://doi.org/10.1007/s11214-018-0574-6

Lognonné, P., Schimmel, M., Stutzmann, E., Davis, P., Drilleau, M., Sainton, G., et al. (2023). Detection of Mars normal modes from s1222 event and seismic noise. *Geophysical Research Letters*. https://doi.org/10.1029/2023GL103205

Maia, J. S., & Wieczorek, M. A. (2022). Lithospheric structure of Venusian crustal plateaus. *Journal of Geophysical Research: Planets*, *127*(2), e2021JE007004. https://doi.org/10.1029/2021je007004

McLennan, S. M. (2022). Composition of planetary crusts and planetary differentiation. In *Planetary volcanism across the solar system* (pp. 287–331). Elsevier.

Moulik, P., Lekic, V., Romanowicz, B., Ma, Z., Schaeffer, A., Ho, T., et al. (2022). Global reference seismological data sets: Multimode surface wave dispersion. *Geophysical Journal International*, *228*(3), 1808–1849. https://doi.org/10.1093/gji/ggab418

O'Rourke, J. G., & Korenaga, J. (2012). Terrestrial planet evolution in the stagnant-lid regime: Size effects and the formation of self-destabilizing crust. *Icarus*, *221*(2), 1043–1060. https://doi.org/10.1016/j.icarus.2012.10.015

Padovan, S., Wieczorek, M. A., Margot, J.-L., Tosi, N., & Solomon, S. C. (2015). Thickness of the crust of mercury from geoid-to-topography ratios. *Geophysical Research Letters*, *42*(4), 1029–1038. https://doi.org/10.1002/2014gl062487

Panning, M. P., Banerdt, W. B., Beghein, C., Carrasco, S., Ceylan, S., Clinton, J. F., et al. (2023). Locating the largest event observed on Mars with multi-orbit surface waves. *Geophysical Research Letters*, *50*(1), e2022GL101270. https://doi.org/10.1029/2022GL101270

Park, J., Vernon, F. L., III, & Lindberg, C. R. (1987). Frequency dependent polarization analysis of high-frequency seismograms. *Journal of Geophysical Research*, *92*(B12), 12664–12674. https://doi.org/10.1029/jb092ib12p12664

Plesa, A.-C., Bozdağ, E., Rivoldini, A., Knapmeyer, M., McLennan, S. M., Padovan, S., et al. (2021). Seismic velocity variations in a 3D Martian mantle: Implications for the insight measurements. *Journal of Geophysical Research: Planets*, *126*(6), e2020JE006755. https://doi.org/10.1029/2020JE006755

Plesa, A.-C., Padovan, S., Tosi, N., Breuer, D., Grott, M., Wieczorek, M., et al. (2018). The thermal state and interior structure of Mars. *Geophysical Research Letters*, *45*(22), 12–198. https://doi.org/10.1029/2018gl080728

Plesa, A.-C., Wieczorek, M., Knapmeyer, M., Rivoldini, A., Walterova, M., & Breuer, D. (2022). Interior dynamics and thermal evolution of Mars–a geodynamic perspective. *Geophysical Exploration of the Solar System*, *63*, 179–230.

Posiolova, L. V., Lognonné, P., Banerdt, W. B., Clinton, J., Collins, G. S., Kawamura, T., et al. (2022). Largest recent impact craters on Mars: Orbital imaging and surface seismic co-investigation. *Science*, *378*(6618), 412–417. https://doi.org/10.1126/science.abq7704

Romanowicz, B. (1987). Multiplet-multiplet coupling due to lateral heterogeneity: Asymptotic effects on the amplitude and frequency of the Earth's normal modes. *Geophysical Journal International*, *90*(1), 75–100. https://doi.org/10.1111/j.1365-246x.1987.tb00676.x

Rost, S., & Thomas, C. (2002). Array seismology: Methods and applications. *Reviews of Geophysics*, *40*(3), 2–1. https://doi.org/10.1029/2000rg000100

Scholz, J.-R., Widmer-Schnidrig, R., Davis, P., Lognonné, P., Pinot, B., Garcia, R. F., et al. (2020). Detection, analysis, and removal of glitches from insight's seismic data from Mars. *Earth and Space Science*, *7*(11), e2020EA001317. https://doi.org/10.1029/2020EA001317

Sori, M. M. (2018). A thin, dense crust for Mercury. *Earth and Planetary Science Letters*, *489*, 92–99. https://doi.org/10.1016/j.epsl.2018.02.033

Stähler, S. C., Khan, A., Banerdt, W. B., Lognonné, P., Giardini, D., Ceylan, S., et al. (2021). Seismic detection of the Martian core. *Science*, *373*(6553), 443–448. https://doi.org/10.1126/science.abi7730

Stähler, S. C., Mittelholz, A., Perrin, C., Kawamura, T., Kim, D., Knapmeyer, M., et al. (2022). Tectonics of cerberus fossae unveiled by marsquakes. *Nature Astronomy*, *6*(12), 1–11. https://doi.org/10.1038/s41550-022-01803-y

Stutzmann, E., Schimmel, M., Lognonné, P., Horleston, A., Ceylan, S., van Driel, M., et al. (2021). The polarization of ambient noise on Mars. *Journal of Geophysical Research: Planets*, *126*(1), e2020JE006545. https://doi.org/10.1029/2020JE006545

Taylor, G. J. (2013). The bulk composition of Mars. *Geochemistry*, *73*(4), 401–420. https://doi.org/10.1016/j.chemer.2013.09.006

van Driel, M., Ceylan, S., Clinton, J. F., Giardini, D., Horleston, A., Margerin, L., et al. (2021). High-frequency seismic events on Mars observed by InSight. *Journal of Geophysical Research: Planets*, *126*(2), e2020JE006670. https://doi.org/10.1029/2020JE006670

Wänke, H., Dreibus, G., Wright, I. P., Cowley, S. W. H., Runcorn, S. K., & Southwood, D. J. (1994). Chemistry and accretion history of Mars. *Philosophical Transactions of the Royal Society of London, Series A: Physical and Engineering Sciences*, *349*(1690), 285–293. https://doi.org/10.1098/rsta.1994.0132

Wieczorek, M. A., Broquet, A., McLennan, S. M., Rivoldini, A., Golombek, M., Antonangeli, D., et al. (2022). Insight constraints on the global character of the Martian crust. *Journal of Geophysical Research: Planets*, *127*(5), e2022JE007298. https://doi.org/10.1029/2022JE007298

Wieczorek, M. A., Neumann, G. A., Nimmo, F., Kiefer, W. S., Taylor, G. J., Melosh, H. J., et al. (2013). The crust of the moon as seen by grail. *Science*, *339*(6120), 671–675. https://doi.org/10.1126/science.1231530

References From the Supporting Information

Clinton, J. F., Ceylan, S., van Driel, M., Giardini, D., Stähler, S. C., Böse, M., et al. (2021). The Marsquake catalogue from InSight, sols 0–478. *Physics of the Earth and Planetary Interiors*, *310*, 106595. https://doi.org/10.1016/j.pepi.2020.106595

Crotwell, H. P., Owens, T. J., & Ritsema, J. (1999). The TauP toolkit: Flexible seismic travel-time and ray-path utilities. *Seismological Research Letters*, *70*(2), 154–160. https://doi.org/10.1785/gssrl.70.2.154

Horleston, A. C., Clinton, J. F., Ceylan, S., Giardini, D., Charalambous, C., Irving, J. C., et al. (2022). The far side of Mars: Two distant marsquakes detected by InSight. *The Seismic Record*, *2*(2), 88–99. https://doi.org/10.1785/0320220007

Plesa, A. C., Grott, M., Tosi, N., Breuer, D., Spohn, T., & Wieczorek, M. A. (2016). How large are present-day heat flux variations across the surface of Mars? *Journal of Geophysical Research: Planets*, *121*(12), 2386–2403. https://doi.org/10.1002/2016JE005126

Stockwell, R. G., Mansinha, L., & Lowe, R. P. (1996). Localization of the complex spectrum: The S transform. *IEEE Transactions on Signal Processing*, *44*(4), 998–1001. https://doi.org/10.1109/78.492555

Taylor, G. J., Stopar, J. D., Boynton, W. V., Karunatillake, S., Keller, J. M., Brückner, J., et al. (2006). Variations in K/Th on Mars. *Journal of Geophysical Research*, *111*(E3), E03S06. https://doi.org/10.1029/2006JE002676

Wieczorek, M. A. (2021). Ctplanet. version 0.2.1. *Zenodo*. https://doi.org/10.5281/zenodo.4439426

Yoshizaki, T., & McDonough, W. F. (2020). The composition of Mars. *Geochimica et Cosmochimica Acta*, *273*, 137–162. https://doi.org/10.1016/j.gca.2020.01.011